

# Effect of pulse current on droplet transfer behavior and weld formation of 304 stainless steel in local dry underwater MIG welding

Haipeng Liao

Wenxu Zhang

Xuyan Li

Kai Pei

Sanbao Lin

Jiyu Tian (✉ [tianjiyu@scut.edu.cn](mailto:tianjiyu@scut.edu.cn))

South China University of Technology <https://orcid.org/0000-0003-1966-7158>

Zhenmin Wang

---

## Research Article

**Keywords:** LDU-PMIG, 304 stainless steel, Peak current, Droplet transfer, Weld formation

**Posted Date:** March 21st, 2022

**DOI:** <https://doi.org/10.21203/rs.3.rs-1452334/v1>

**License:** © ⓘ This work is licensed under a Creative Commons Attribution 4.0 International License. [Read Full License](#)

---

# Abstract

In this study, 304 stainless steel which widely used in the industrial field due to its excellent thermostability, corrosion resistance and welding performance, was welded using local dry underwater pulse metal inert-gas (LDU-PMIG) welding technology. The effect of different pulse peak currents on droplet transfer behavior and weld formation was studied. The results show that short circuit transfer, globular transfer, and projected transfer could be observed in the LDU-PMIG process. With the peak current of 240A, the droplet transfer mode was short circuit transfer and globular transfer, the weld formation was irregular with large particle spatters around the weld. With the peak current increased to 260A, the droplet transfer mode changed into the globular transfer, and the weld formation quality was improved. With the peak current of 280A, the droplet transfer mode was projected transfer, the weld formation was satisfied with few spatter, and the coefficient of weld formation was the largest, projected transfer was the most stable mode. With the increase of the peak current from 300A to 320A, the droplet transfer mode did not change, but the instability of the welding arc resulted in poor weld formation with serious spatters and undercuts.

## 1 Introduction

304 stainless steel exhibits the advantages of significant corrosion resistance and excellent mechanical property, which has been widely used in the marine environment, oil and gas industries, and nuclear sector [1]. Underwater welding is one of the most significant technology for manufacturing and repairing 304 stainless steel structures in the marine equipment, including offshore drilling platform, marine engineering vessel, offshore wind power and nuclear power plant [2]. Underwater welding technique mainly includes wet welding, dry welding and local dry welding [3]. Among them, local dry underwater welding (LDUW) has gradually become a research hotspot in the field of underwater welding due to high flexibility, good adaptability, low cost, and good weld formation [4–5].

In LDUW, the drainage device is adopted to drain the water around the welding area to provide a stable local dry cavity for underwater welding, which is similar to the condition of on-land welding [6]. Recently, researchers have conducted a great deal of research on LDUW. Di et al. [7] used a drainage device to carry out welding experiments in LDUW successfully and concluded that the rapid cooling effect of underwater environment could improve the impact toughness and tensile strength of welds. Hu et al. [8] obtained duplex stainless steel welded joints under different simulated water depths by adopting local dry welding technique and revealed that the austenite content of the weld joints increased initially and decreased afterwards. Han et al. [9] designed a micro-drain cover based on the shrinkage nozzle principle with a dual air curtain structure and carried out a series of experiments, they reported that the micro-drain cover could ensure the stability of welding process and the good quality of weld formation.

Pulse metal inert-gas welding is an efficient welding method with low average input current, which is suitable for all-directional welding of aluminum, magnesium, copper and stainless steel, etc., it can control the stability of droplet transfer and obtain excellent weld formation. Hence, the combination of LDUW welding method and pulsed MIG technique (LDU-PMIG) has broad application prospect and important engineering application value.

Welding current has a significant impact on the welding process [10], which is mainly reflected in changing the heat input and the stability of welding process, these factors will greatly affect the quality of weld formation. Guo et al. [11] explored the effect of pulse current on the stability of welding process and weld formation in FCAW, they demonstrated that the stable mass transfer process and welding arc could increase the efficiency of heat input, decreased the acicular ferrite content and increased the pre-eutectoid ferrite content in welds, the hardness and tensile strength of welds were similar to the in-air weld. Singh et al. [12] studied the effect of welding current on the weld formation in tungsten inert gas welding. They put forward that with the increases of welding current, the weld penetration, weld width, and weld reinforcement all increased. Tabrizi et al. [13] researched the effect of pulse and continuous current on the mechanical performance of AISI 316L stainless steel joints in gas tungsten arc welding. They drew a conclusion that the welded joints under pulse current mode had higher hardness and toughness. Karunakaran et al. [14] analyzed the effect of pulse current on the mechanical properties and microstructure characteristics of aluminum alloy joints welded by gas tungsten arc welding technique, they revealed that pulse current welding could improve the tensile strength of welds. However, researchers mainly focus on the analysis of weld formation quality for the effect of welding current on the welding process, few studies have concentrated on droplet transfer for that.

There are many modes of droplet transfer in MIG welding process, the transfer modes have a significant influence on weld formation quality [15–16]. Therefore, researchers have conducted many studies on droplet transfer in welding process. Ma et al. [17] investigated the influence of the main arc voltage on arc behavior and droplet transfer in tri-arc twin wire welding. It indicated that with the increase of the main arc voltage, the droplet transfer changed from an unstable mixing transfer to a stable repulsion particle transfer. Wang et al. [18] explored the effect of ultrahigh-frequency on arc behavior and droplet transfer. Through experiments and theoretical analysis, they verified that ultrahigh-frequency pulse alternating current cold metal transfer arc exhibited a good stability, with the pulse frequency increased from 60 to 80 kHz, the length of welding arc and the droplet diameter were maintained within an optimum range. Yang et al. [19] studied the influence of wire feeding speed on droplet transfer and weld formation in GMAW for high nitrogen austenitic stainless steel. The results revealed that stable short circuit transfer, unstable short circuit transfer and spray transfer would be observed in the process, the weld formation for stable short-circuit transfer was the best quality with few spatters. Cai [20] supplied Ar and He alternately as shielding gas in MIG welding for 5A06 aluminum alloy, they found that when the shielding gas was alternately supplied, the welding current fluctuated and the droplet transfer mode would change alternately. Wang et al. [21] studied the effect of pulse frequency on droplet transfer and weld formation in MIG welding. They demonstrated that with the increase of pulse frequency, the frequency of droplet transfer decreased. In the existing studies, there is little research about the effect of pulse peak current on droplet transfer behavior in the process of LDU-PMIG. Therefore, it is difficult to explain the effect of pulse current on the quality of weld formation from the perspective of droplet transfer behavior.

In this study, LDU-PMIG experiments were performed under different pulse currents, by processing the electrical signals and droplet transfer images, the effects of pulse currents on droplet transfer and weld formation quality in the LDU-PMIG welding technique were investigated.

## 2 Experimental Procedure

The test platform of LDU-PMIG is mainly composed of the welding robot, underwater welding power supply with the rated power of 15kW, wire feeder, micro-drainage device, image capturing device, electrical signal acquisition device and gas supply device, as shown in Fig. 1. Image capturing device includes the dysprosium lamp with the power of 1.8kW and the high-speed camera with a frame rate of 2000 fps, which can be used to capture the images of droplet transfer during the welding process. The electrical signal acquisition device includes Hall sensor and oscilloscope, which can be adopted to detect welding current and voltage parameters during the welding process.

The welding material was AISI 304 stainless steel plate with a dimension of 300mm×100mm×5mm. The welding wire was selected as 308Lsi with the diameter of 1.2 mm. To ensure the exploratory experiments under the pulse current process parameters can be carried out successfully, multiple groups of pre-experiments were conducted. Considering the welding process stability and weld formation quality, the exploration range of peak current was set from 240A to 320A. The welding robot was employed to perform the overlay welding experiments on the 304 stainless steel plate, the welding process was operated in a transparent water tank with a depth of 200mm. The welding parameters are shown in Table 1. A mixed gas of 98% Ar and 2% CO<sub>2</sub> was used as the shielding gas and drainage gas. Compared with traditional on-land MIG welding, LDU-PMIG technique has a more complicated welding process due to the effect of rapid water cooling and larger gas flow. To avoid the huge interference of the complex underwater environment in the experiments, each group of pulse current parameters was carried out three times to reduce the errors.

Table 1  
Parameters of welding test.

| Group | Base current(A) | Peak current(A) | Pulse frequency (Hz) | Peak current duty cycle | Welding speed (mm/s) | Drainage gas pressure(MPa) | Shielding gas pressure(MPa) |
|-------|-----------------|-----------------|----------------------|-------------------------|----------------------|----------------------------|-----------------------------|
| A     | 100             | 240             | 100                  | 32%                     | 15                   | 0.2                        | 0.2                         |
| B     | 100             | 260             | 100                  | 32%                     | 15                   | 0.2                        | 0.2                         |
| C     | 100             | 280             | 100                  | 32%                     | 15                   | 0.2                        | 0.2                         |
| D     | 100             | 300             | 100                  | 32%                     | 15                   | 0.2                        | 0.2                         |
| E     | 100             | 320             | 100                  | 32%                     | 15                   | 0.2                        | 0.2                         |

After conducting the welding experiments, the electrical signals detected were processed to obtain the U-I diagrams, the stability of droplet transfer process was studied. The droplet transfer videos were edited into pictures to investigate the droplet transfer under different peak current parameters. A stereo microscope was adopted to detect the dimensions of the weld cross-section when the welds were cut, sampled, polished, and corroded. The corrosive solution was composed of picric acid, nitric acid and ethyl alcohol. In addition, the mechanical model of droplet transfer was established to explain the formation mechanism for different droplet transfer modes and explore the influence of the droplet impact force on weld penetration.

## 3 Results And Discussions

### 3.1 Stability analysis of welding process

The U-I diagrams under each peak current were obtained as shown in Fig. 2. The trajectory of working points during the welding process can be clearly observed, and the concentration degree of working points can reflect the stability of welding current and voltage [22].

The U-I diagram of 240A is illustrated in Fig. 2a, three typical arc state regions could be observed, including arc-extinguishing region (I), short-circuit region (II) and arc-burning region (III). In arc-extinguishing region, the welding peak current was too inadequate to guarantee the stability of arc combustion. In short-circuit region, the droplet with welding wire was contacted with the molten pool before it separated from welding wire and caused the short circuit. At this moment, the arc voltage was small and the arc length was very short. Due to the voltage detected was the output voltage of the welding power source, which was related to the welding wire, cable and other resistances, therefore the welding voltage would not reach zero. The occurrence of arc extinguishing and short circuit led to the extreme instability of the electrical parameters, which was not conducive to the stable arc burning. The U-I diagram under 260A is shown in Fig. 2b, the arc-extinguishing region and the short-circuit region disappeared and the stability of welding process was improved. The U-I diagram of 280A is shown in Fig. 2c. The welding voltage and current of the welding process had the least fluctuations, which indicating the arc stability of this parameter was the most satisfied. In the arc-burning region under this current, it could be observed that the U-I signal had an obvious circuit, A, B, C, and D region were respectively the base current stage, the climbing stage from the base current to the peak current, the peak current stage and the falling stage from the peak current to the base current. With the peak current increased from 280A to 320A, the electrical parameters became unstable, that was because with the peak current increasing, the gap between the peak and base current became larger, welding current frequently climbed vertically from the base current to the peak current, and then dropped vertically from the peak current to the base current, which would inevitably lead to violent fluctuations of welding arc.

### 3.2 Droplet transfer modes under different peak currents

Stable droplet transfer process is the essential for high stability welding process. Therefore, it is necessary to study the droplet transfer process under different peak current parameters and clarify the correlation systems between pulse currents and droplet transfer modes. With the peak current increased, three types of droplet transfer modes occurred in the welding process, that were short circuit transfer, globular transfer and projected transfer.

#### 3.2.1 Short circuit transfer

Small peak current leads to the insufficiency of heat input at the peak stage, resulting that the wire feeding speed is greater than the melting speed of welding wire, the droplet with welding wire entered the molten pool early before separating from welding wire. The whole process of droplet transfer takes place inside the molten pool, which forms the short circuit transfer. When the peak current was 240A, the droplet transfer modes were short circuit transfer and globular transfer. The short circuit transfer process is illustrated in Fig.

3. At the beginning, the welding wire was continuously fed into the molten pool, no obvious droplet was observed at this moment. After 14ms, a distinct droplet was developing, and then the droplet grown up and began to approach the molten pool. At 18ms, the welding wire with large droplet contacted directly with the molten pool, which formed the short circuit transfer. The arc voltage decreased rapidly and the arc light disappeared, only the appearance of the droplet could be observed, and the arc reignited at 24.5ms. When short circuit transfer was in process, the arc voltage decreased rapidly, while the welding current increased sharply. The whole process could be matched with the electrical signal detected by acquisition system, as shown in Fig. 4, it can be seen that the electrical parameters under short circuit transfer mode were extremely unstable, the current curve had a huge peak, which was not conducive to welding process.

### **3.2.2 Globular transfer**

When the peak current is small, the surface tension of droplet prevents the droplet separating from welding wire, results in metal accumulation at the root of the welding wire. At this moment, the droplet volume continuously increases. Then the droplet detaches from the welding wire under the action of gradually increasing gravity, which forms the globular transfer. Figure 5 illustrates the process of globular transfer with the peak current of 260A. In the initial moment, it could be clearly observed that the droplet gradually grown up at the root of welding wire. The droplet began to separate from the wire at 5ms, and then it kept a regular spherical shape. At 11ms, the droplet transferred smoothly to the molten pool. At 15ms, the droplet was contacted with the molten pool and the globular transfer process was completed. Figure 6 shows the output current and voltage waveforms of 260A, the fluctuations of the electrical signals were small, and the smooth globular droplet transfer mode can be obtained under this process parameter.

### **3.2.3 Projected transfer**

With the further increase of peak current, the arc force generated by welding current makes the droplet separate from welding wire before it grows up, and the droplet shoots into molten pool at a high speed, which forms the projected transfer. When the peak current increased from 280A to 320A, the droplet transfer mode was projected transfer. Figure 7 illustrates the whole process of droplet transfer with the peak current of 280A. After separating from welding wire, the overall shape of droplet was a regular ellipsoid. At 2ms, it could be clearly observed that two droplets existed at the same time, and the droplets quickly dropped into the molten pool. It took 6ms to complete the whole transfer process, which was generally the mode of many droplets in one pulse cycle. The diameter of the droplet was significantly decreased, and the dropping speed increased. According to the droplet transfer images and the output electrical signal waveforms of 280A (Fig. 8), projected transfer was the most satisfied droplet transfer mode.

## **3.3 Weld formation characteristics**

Figure 9 illustrates the weld formation of different peak currents. When the peak current was 240A, the transfer mode was short circuit transfer and globular transfer. Among them, the short circuit transfer mode was extremely unstable, and droplet exploding would generate many explosive spatters during the transfer process, resulting in uneven weld formation with large particle spatters around the welds. With the peak current increased to 260A, the short circuit transfer disappeared, and the droplet transfer mode was globular transfer. Compared with short circuit transfer, this mode was more stable. On the action of the arc force

generated by welding arc, the droplet would deviate from the welding wire during the transfer process, causing that part of droplet deviated from the molten pool, but the overall weld formation quality was improved. When the peak current was 280A, the droplet transfer mode was projected transfer, and the droplet dropped into molten pool stably and quickly, which contributed to obtain high weld formation quality with satisfied continuity and smoothness. This droplet transfer mode was the most stable. When the peak current increased from 300A to 320A, the transfer form was still projected droplet transfer. With the heat input further increased, the droplet dropping speed increased and the droplet diameter decreased. The instability of arc voltage caused irregular droplet dropping, which led to worse weld formation with some small particle spatters and undercuts.

Furthermore, to explore the influence of peak current on weld formation quality further, dimension detections were carried out on the cross section of the welds, and the weld penetration (H), weld width (B) and weld reinforcement (h) could be obtained. Figure 10 illustrates the cross-sectional morphology of the weld of 260A.

The coefficient of weld formation is the ratio of the weld width (B) to the weld penetration (H), which can be used to measure the weld formation quality. Three sets of sectional dimension data under each peak current parameter were detected and collected, and the average values and standard deviations of each sectional dimension were obtained. Figure 11 illustrates that with the increase of the peak current, the weld width, weld penetration, and weld reinforcement increased, and the coefficient of weld formation first increased and then decreased. The coefficient of weld formation of 280A was the largest. The error bar in Fig. 11 represented the standard deviation of each parameter. When the peak current was small, three unstable factors, including short circuit, arc interruption and reignition, inevitably resulting in unstable droplet transfer. And with the peak current increased, the arc length increased, the droplet size decreased, and the dripping speed increased. Being subjected to the large arc force, the droplet transfer became disordered, which caused the inconformity of several sets of cross-sectional parameters of the same weld.

The increase of heat input would lead to the increase of weld penetration. But the strong water cooling effect caused by the contact between the rear face of base metal and water would lead to rapid cooling of the molten pool, which would inhibit the increase of weld penetration. In addition, the increase of the heat input would help to increase the weld width. However, with the increase of weld penetration, the arc length remained unchanged because the welding voltage did not change. When the arc dived into the molten pool, the decrease of arc swing angle would weaken the tendency increase of weld width and limit the growth speed of weld width. Besides, the increase of peak current made the increase of welding wire melting speed, which caused the increase of weld reinforcement accordingly. Therefore, it could be found that with the current increased, the growth extent of weld width and weld penetration increased first and then decreased, for the reason that the increase extent of weld width was greater than what of weld penetration, the coefficient of weld formation increased initially and decreased afterwards.

### **3.4 Mechanical modelling and analysis of droplet transfer**

### 3.4.1 Formation mechanism of different droplet transfer modes

To profoundly explain the influence of different pulse currents on different droplet transfer modes, the mechanical model of droplet transfer was established and studied. Figure 12 illustrates the mechanical model of the droplet growing at the root of welding wire. According to the static equilibrium theory [23], the droplet is subjected to gravity  $G$ , surface tension  $F_s$ , plasma flow force  $F_p$  and electromagnetic force  $F_{em}$ . The direction of gravity, plasma force and electromagnetic force is downward, these forces promote the droplet transfer to the molten pool, and the direction of surface tension is upward, which maintains the droplet shape and prevents the droplet breaking away from the wire.

As the welding wire melting, the droplet grows up gradually and causes the increase of droplet gravity. The calculation method of gravity is given by:

$$G = \frac{\pi D_0^3 \rho g}{6}$$

1

Where  $D_0$  stands for the droplet diameter,  $\rho$  is the droplet density, and  $g$  represents the gravitational acceleration. Before separating from welding wire, the droplet would adhere to the welding wire due to surface tension, which can be expressed as:

$$F_s = \pi d_0 \gamma$$

2

Where  $d_0$  is the diameter of welding wire;  $\gamma$  is the surface tension coefficient. The coefficient will change with temperature, which depends on the welding current [24]. The relationship between surface tension coefficient  $\gamma$  and welding current  $I$  can be expressed by:

$$\gamma = -0.0216 \times e^{\frac{I}{43.517}} + 4.11379$$

3

Eq. (3) reveals that with the increase of welding current, the surface tension coefficient will decrease. During the welding process, the conical welding arc makes the arc force different on the different section, resulting in a pressure difference. Axial thrust caused by the pressure difference prompts shielding gas to flow from the root of welding wire to the molten pool, forming the plasma flow force [25], which provides thrust to drive the droplet move towards the workpiece along the axis. The plasma flow force can be expressed as:

$$F_p = A_p C_d \pi \frac{p_f v_f^2}{2}$$

4

Where  $A_p$  is the action area of plasma flow force,  $C_d$  is the tension coefficient of plasma flow force,  $\rho_f$  is the density of plasma, that is the density of shielding gas;  $v_f$  is plasma flow rate.

In the MIG welding process, electric field and magnetic field generated by the welding current flow will provide electromagnetic force  $F_{em}$  to the droplet, which can be expressed:

$$F_{em} = \frac{\mu_0 I^2}{4\pi} \left[ \ln \frac{D_0 \sin \theta}{d_0} + \frac{2}{(1 - \cos \theta)^2} \times \ln \frac{2}{1 + \cos \theta} - \frac{1}{1 - \cos \theta} - \frac{1}{4} \right]$$

5

Where  $\mu_0$  is the vacuum permeability and  $\theta$  is the arc root angle.

The resultant force  $F$  on the droplet can be expressed as:

$$F = G + F_p + F_{em} - F_s$$

6

When the peak current is small, the surface tension  $F_s$  plays a dominant role in Eq. (6), causing that the resultant force  $F$  keeps less than zero, and the droplet cannot separate from welding wire, which forms short circuit transfer. With the peak current increases, the surface tension  $F_s$  decreases, the welding wire melting prompts the droplet to develop adequately. At this time, the gravity  $G$  is in the leading position, making the resultant force  $F$  be more than zero, the droplet will separate from the welding wire, which forms globular transfer. With the peak current further increases, the electromagnetic force  $F_{em}$  will increase and become the most significant factors, causing the resultant force  $F$  be more than zero, the droplet will separate from welding wire before it grown up, which forms projected transfer.

### 3.4.2 The effect of impact force on weld penetration

To further explore the influence of peak current on weld penetration, it is necessary to calculate the momentum and impact force of the droplet before it falls into the molten pool. When obtaining the droplet transfer images, the droplet diameter under different peak current can be calculated. Because of the same size of each picture, the welding wire diameter  $d_0$  of 1.2mm can be regarded as the reference substance.

As shown in Fig. 13,  $d_1$  and  $D_1$  stand for the welding wire diameter and droplet diameter respectively, which measured by the picture, the actual droplet diameter  $D_0$  can be calculated:

$$D_0 = \frac{D_1 d_0}{d_1}$$

7

Then, the droplet mass  $m$  can be expressed:

$$m = \frac{\pi \rho D_0^3}{6}$$

8

The high-speed camera can be employed to capture the droplet transfer images with the frame rate of 2000 fps, and the time interval  $T$  of each picture is 0.5ms. Selecting three pictures of the droplet before falling into the molten pool, as shown in Fig. 13. According to the method of welding wire diameter reference, the displacement difference of three pictures can be obtained as  $h_1$  and  $h_2$  respectively, and the velocity  $v$  and acceleration  $a$  of the droplet before entering the molten pool are approximately calculated by:

$$v = \frac{h_1 + h_2}{2T}$$

9

$$a = \frac{h_2 - h_1}{T^2}$$

10

According to Eqs. (7), (9) and (10), the actual diameter, velocity and acceleration of the droplet under different peak currents were calculated, as shown in Fig. 14. It reveals that with the peak current increased, the diameter of the droplet decreased, and the speed and acceleration of the droplet increased.

Then, the momentum  $p$  and the impact force  $Q$  of the droplet can be expressed:

$$p = mv = \frac{\pi\rho D_0^3(h_1 + h_2)}{12T}$$

11

$$Q = ma = \frac{\pi\rho D_0^3(h_2 - h_1)}{6T^2}$$

12

Hence, the effect of momentum and impact force of droplet on weld penetration under different peak currents could be explained as shown in Fig. 15. With the peak current increased, the droplet diameter decreased, the droplet velocity increased, these two factors made the decrease of droplet momentum. Figure 15a shows that the weld penetration increased with the decrease of droplet momentum. It is obviously unreasonable to adopt droplet momentum as a reference for determining the weld penetration. Figure 15b illustrates that the impact force of droplet falling into the molten pool increased continually and had an evident positive effect on the weld penetration, that was, the greater the impact force, the deeper the weld penetration. Consequently, the droplet impact force can be regarded as the reference for determining the weld penetration.

## 4 Conclusions

In this study, several sets of LDU-PMIG welding experiments under different pulse currents(240A ~ 320A) were conducted, the electrical parameters, droplet transfer images, and weld formation quality during the welding process were investigated, then the mechanical model of the droplet transfer was established and studied. The conclusions are summarized as follows:

- (1) With the peak current increased, the droplet transfer modes changed from short circuit transfer and globular transfer (240A) to globular transfer (260A), then to projected transfer (280A ~ 320A). Projected transfer was the most stable mode.
- (2) With the peak current of 280A, the output electrical signals were ordered with the least fluctuates. The weld formation was satisfied with smoothness, uniformity and absence of spatters and undercuts, and the coefficient of weld formation was the largest.
- (3) The mechanical model of droplet transfer revealed that with the peak current increased, the surface tension, gravity, electromagnetic force would respectively take the leading place, which severally led to short circuit transfer, globular transfer and projected transfer.
- (4) With the peak current increased, the droplet diameter decreased, the droplet velocity and droplet impact force increased, but the droplet momentum decreased. The impact force had an extremely positive effect on the weld penetration, which could be adopted as the reference for determining the weld penetration.

## Declarations

**Acknowledgements** The authors are thankful to editors and reviewers.

**Author contribution** Haipeng Liao: conceptualization; original draft preparation; review and editing the manuscript; supervision. Wenxu Zhang: investigation and summary of partial content in the manuscript. Xuyan Li: investigation and data curation. Kai Pei: investigation and data extraction of partial content in the manuscript. Sanbao Lin: experiment, supervision, methodology. Jiyu Tian: writing, review and editing. Zhenmin Wang: funding acquisition; conceptualization; and editing.

**Funding** This work was supported by the National Natural Science Foundation of China [Grant number U2141216, Grant number 51875212,]; State Key Lab of Advanced Welding and Joining, Harbin Institute of Technology [Grant number AWJ21Z03]; Key Technical Projects of Shenzhen City [Grant number JSGG20201201100401005, Grant number JSGG20201201100400001]; Marine Economic Development (Six Marine Industries) Special Funding Project of Guangdong Province [Grant number GDNRC[2021]46]; Science and Technology Planning Project of Guangdong Province [Grant number 2021B1515420006] .

**Data availability** The datasets generated and/or analyzed during the current study are available from the corresponding author on reasonable request.

**Ethics approval** The authors declare that this manuscript was not submitted to more than one journal for simultaneous consideration. Also, the submitted work was original and has not been published elsewhere in any form or language.

**Consent to participate and publish** The authors declare that they participated in this paper willingly and the authors declare to consent to the publication of this paper.

**Competing interests** The authors declare no competing interests.

**Informed consent** All the authors listed have approved the manuscript that is enclosed.

## References

1. Li J, Sun Q, Liu Y et al (2020) Melt flow and microstructural characteristics in beam oscillation superimposed laser welding of 304 stainless steel. *J Manuf Process* 50:629–637. <https://doi.org/10.1016/j.jmapro.2019.12.053>
2. Fu YL, Guo N, Cheng Q et al (2020) Underwater laser welding for 304 stainless steel with filler wire. *J Mater Res Technol* 9(6):15648–15661. <https://doi.org/10.1016/j.jmrt.2020.11.029>
3. Sehgal AK (2021) An investigation of variable welding current on impact strength of metal inert gas welded specimen. *Materials Today: Proceedings* 37:3679–3682. <https://doi.org/10.1016/j.matpr.2020.10.151>
4. Sun K, Zeng M, Shi YH et al (2018) Microstructure and corrosion behavior of S32101 stainless steel underwater dry and wet welded joints. *J Mater Process Technol* 256:190–201. <https://doi.org/10.1016/j.jmatprotec.2018.02.018>
5. Fydrych D, Rogalski G (2013) Effect of underwater local cavity welding method conditions on diffusible hydrogen content in deposited metal. *Weld Int* 27(3):196–202. <https://doi.org/10.1080/09507116.2011.600033>
6. Zhai YL, Yang LJ, He TX et al (2017) Weld morphology and microstructure during simulated local dry underwater FCTIG. *J Mater Process Tech* 250:73–80. <https://doi.org/10.1016/j.jmatprotec.2017.07.010>
7. Di XJ, Ji SX, Cheng FJ et al (2015) Effect of cooling rate on microstructure, inclusions and mechanical properties of weld metal in simulated LDUW. *Mater Des* 88:505–513. <https://doi.org/10.1016/j.matdes.2015.09.025>
8. Hu Y, Shi YH, Sun K et al (2019) Microstructure evolution and mechanical performance of underwater local dry welded DSS metals at various simulated water depths. *Journal of Materials Processing Technology* 264:366–376. <https://doi.org/10.1016/j.jmatprotec.2018.09.023>
9. Han LG, Wu XM, Chen GD et al (2019) LDUW of 304 stainless steel based on a microdrain cover. *J Mater Process Technol* 268:47–53. <https://doi.org/10.1016/j.jmatprotec.2018.12.029>
10. Shi YH, Wang GR (2006) Vision based seam tracking system for underwater flux cored arc welding. *Science and Technology of Welding and Joining*. 11:271–277. <https://doi.org/10.1179/174329306x102084.3>
11. Guo N, Cheng Q, Fu YL et al (2019) Investigation on the mass transfer control, process stability and welding quality during underwater pulse current FCAW for Q235. *J Manuf Process* 46:317–327. <https://doi.org/10.1016/j.jmapro.2019.08.022>

12. Singh RP, Agrawal MK (2021) Effect of welding current on the dimensions of bead in tungsten inert gas welding process. *Materials Today: Proceedings* 45:3235–3239. <https://doi.org/10.1016/j.matpr.2020.12.382>
13. Tabrizi TR, Sabzi M, Anijdan SHM et al (2021) Comparing the effect of continuous and pulsed current in the GTAW process of AISI 316L stainless steel welded joint: microstructural evolution, phase equilibrium, mechanical properties and fracture mode. *J Mater Res Technol* 15:199–212. <https://doi.org/10.1016/j.jmrt.2021.07.154>
14. Karunakaran N, Balasubramanian V (2021) Effect of pulsed current on temperature distribution, weld bead profiles and characteristics of gas tungsten arc welded aluminum alloy joints. *Trans Nonferrous Met Soc China* 21:278–286. [https://doi.org/10.1016/S1003-6326\(11\)60710-3](https://doi.org/10.1016/S1003-6326(11)60710-3)
15. Kang S, Kang M, Jang YH et al (2020) Droplet transfer and spatter generation in DC–AC pulse tandem gas metal arc welding. *Science and Technology of Welding and Joining* 25(7):589–599. <https://doi.org/10.1080/13621718.2020.1786262>
16. Cai XY, Fan CL, Lin SB et al (2016) Effects of shielding gas composition on arc characteristics and droplet transfer in tandem narrow gap GMA welding. *Sci Technol Weld Joining* 22(5):1–8. <https://doi.org/10.1080/13621718.2016.1253535>
17. Ma Z, Zhuang MH, Li MQ (2020) Effect of main arc voltage on arc behavior and droplet transfer in tri-arc twin wire welding. *J Mater Res Technol* 9(3):4876–4883. <https://doi.org/10.1016/j.jmrt.2020.03.007>
18. Wang DL, Wu CF, Suo YC et al (2019) Effect of pulse frequency on arc behavior and droplet transfer of 2198 Al–Li alloy by ultrahigh-frequency pulse AC CMT welding. *J Mater Res Technol* 8(5):3950–3958. <https://doi.org/10.1016/j.jmrt.2019.07.003>
19. Yang DQ, Xiong HY, Huang Y et al (2021) Droplet transfer behavior and weld formation of gas metal arc welding for high nitrogen austenitic stainless steel. *J Manuf Process* 65(3):491–501. <https://doi.org/10.1016/j.jmapro.2021.03.048>
20. Cai XY, Lin SB, Wang BZ (2020) Droplet transfer and weld formation of MIG welding with Ar-He alternating gas for aluminum alloy. *J Manuf Process* 49:94–101. <https://doi.org/10.1016/j.jmapro.2019.11.012>
21. Wang ZM, Pei K, Han LG et al (2021) Effect of pulse frequency on droplet transfer and weld formation in LDUW. *J Manuf Process* 68:1726–1734. <https://doi.org/10.1016/j.jmapro.2021.06.065>
22. Ma Q, Luo CC, Liu SX et al (2021) Investigation of arc stability, microstructure evolution and corrosion resistance in underwater wet FCAW of duplex stainless steel. *J Mater Res Technol* 15:5482–8492. <https://doi.org/10.1016/j.jmrt.2021.11.023>
23. Zhang SY, Ma GH, Peng XF et al (2017) Numerical simulation of the effects of bypass current on droplet transfer during AZ31B magnesium alloy DE-GMAW process based on FLUENT. *Int J Adv Manuf Technol* 90(1–4):857–863. <https://doi.org/10.1007/s00170-016-9438-y>
24. Ding XP, Li H, Yang LJ et al (2013) Numerical simulation of metal transfer process in tandem GMAW. *Int J Adv Manuf Technol* 69(1–4):107–112. <https://doi.org/10.1007/s00170-013-4999-5>

25. Ma GH, Liu JC, Yu LS et al (2019) Numerical simulation of droplet transfer process in ultrasonic-assisted MIG welding. Sci Technol Weld Joining 25(3):1–11.  
<https://doi.org/10.1080/13621718.2019.1664540>

## Figures

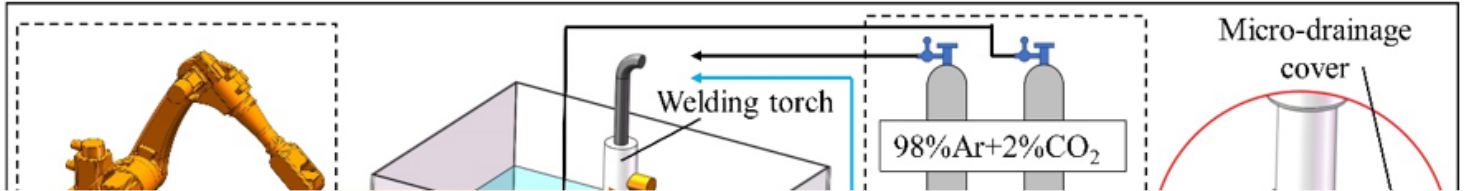


**Figure 1**

Schematic diagram of LDU-PMIG test platform.

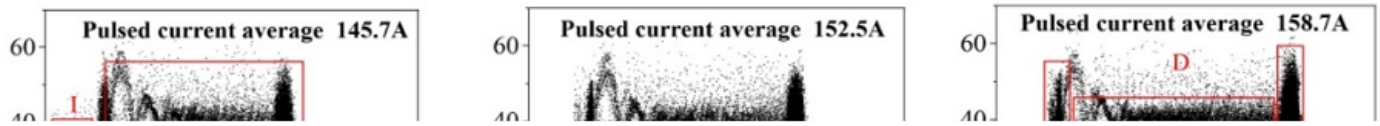


Figure 2

U-I diagrams of different peak currents.

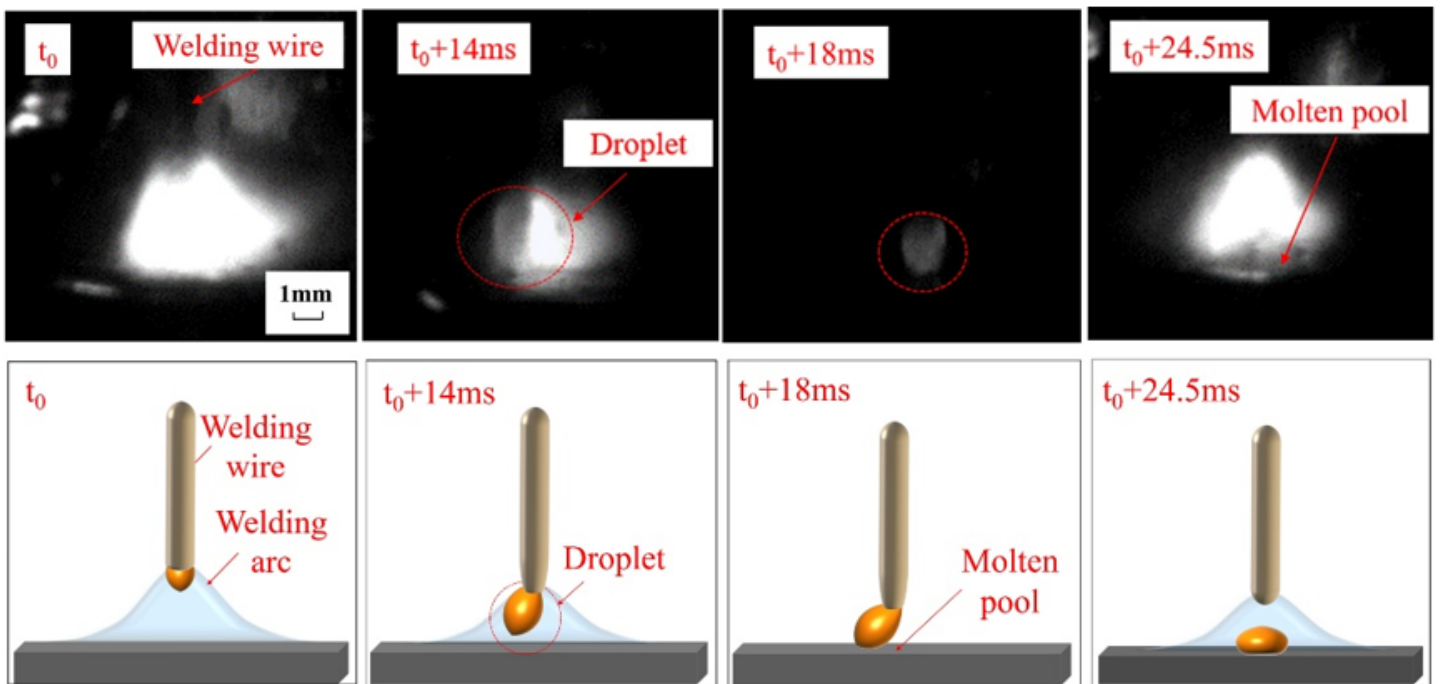
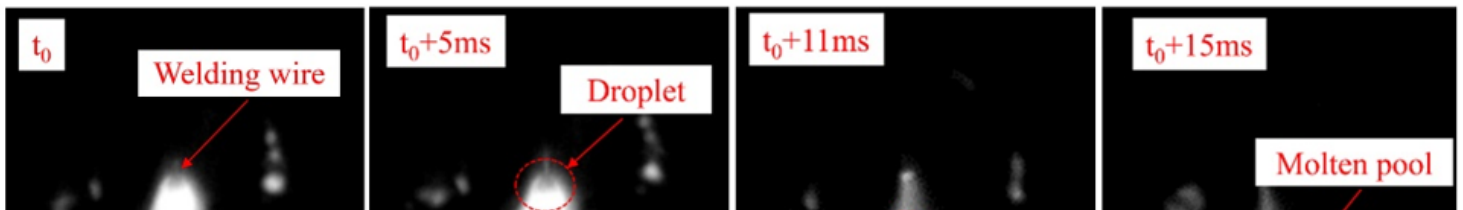


Figure 3

Short circuit transfer process at the peak current of 240A.

**Figure 4**

The output current and voltage waveforms of 240A.



**Figure 5**

Globular transfer process with the peak current of 260A.

**Figure 6**

The output current and voltage waveforms of 260A.

**Figure 7**

Projected transfer process with the peak current of 280A.

### Figure 8

The output current and voltage waveforms of 280A.



### Figure 9

Weld formation of different peak currents: (a)240A; (b)260A; (c)280A; (d)300A; (e)320A.

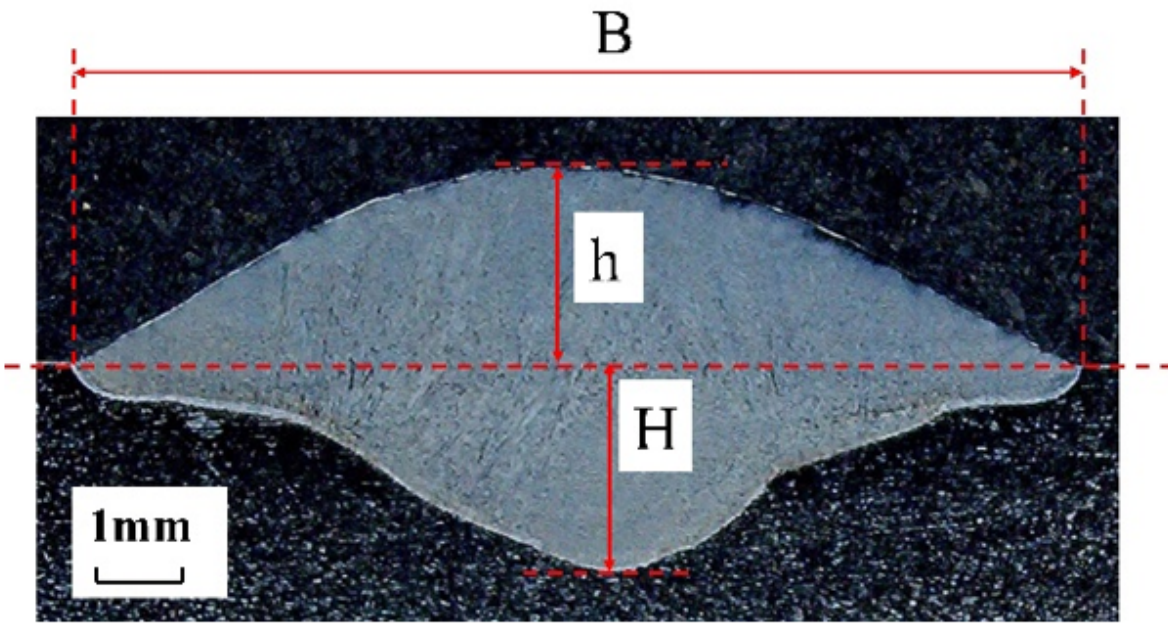
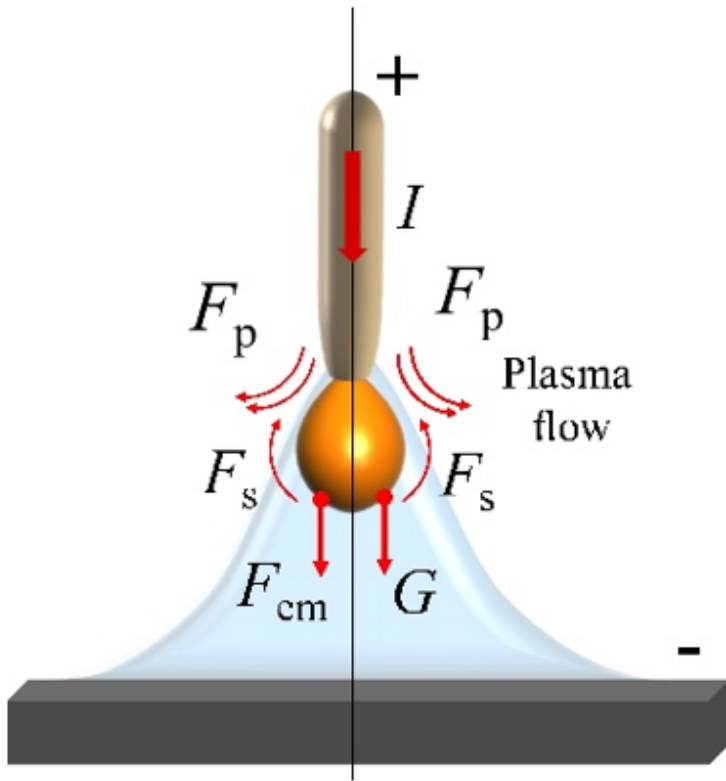


Figure 10

Cross-sectional morphology of the weld with peak current of 260A.

Figure 11

Weld dimensions of different peak currents.



**Figure 12**

Mechanical model of droplet growth stage.

**Figure 13**

Solution schematic diagram of droplet diameter, velocity and acceleration.

**Figure 14**

Droplet diameter, velocity and acceleration of different peak currents.

**Figure 15**

Effect of momentum and impact force on weld penetration: (a) momentum; (b) impact force.